Volume 5
Number 21
7 November 2024
Pages 8321–8732

Materials Advances

rsc.li/materials-advances

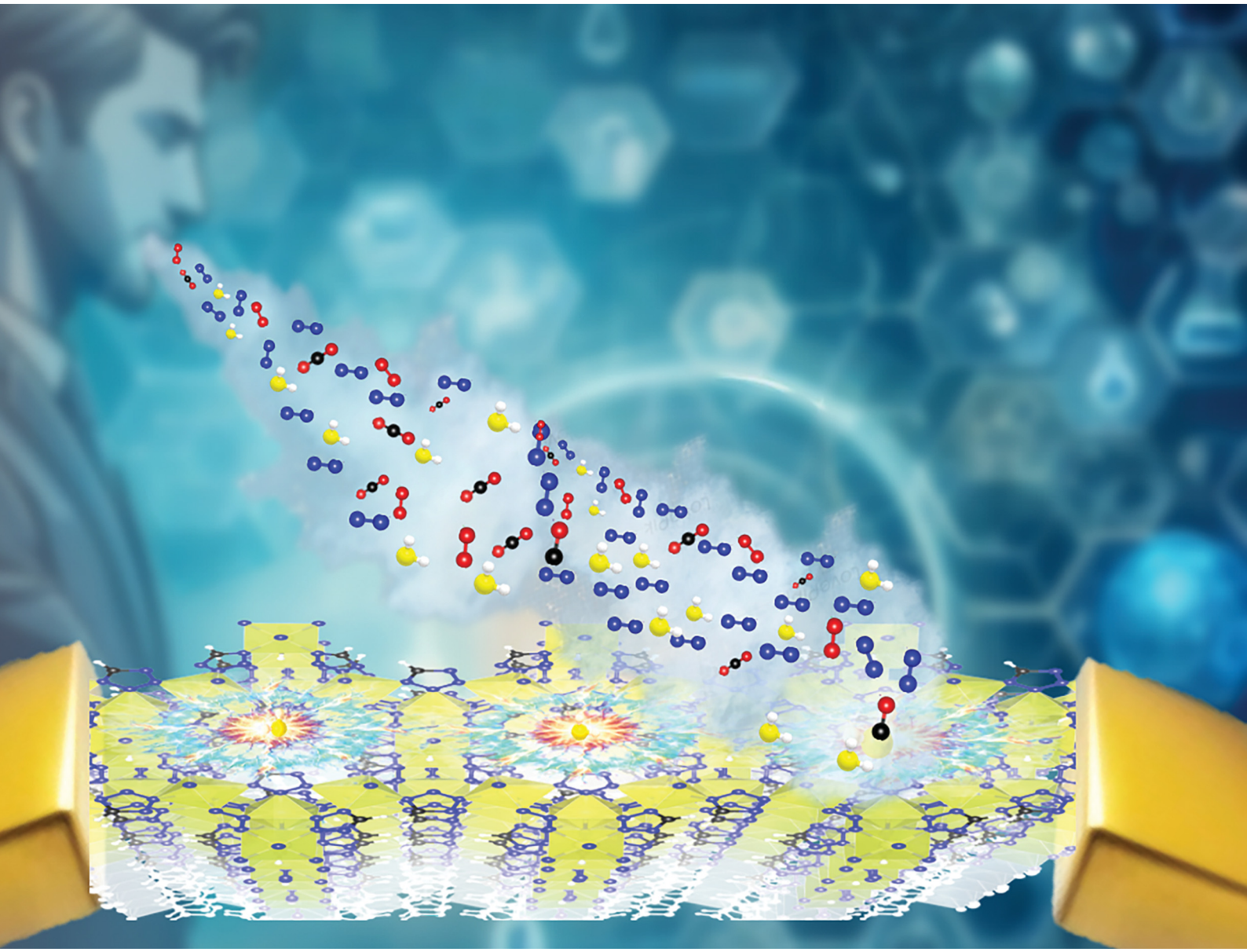

ISSN 2633-5409

ROYAL SOCIETY OF CHEMISTRY

COMMUNICATION

Khaled N. Salama, Mohamed Eddaoudi *et al.*
A non-invasive approach for H_2S gas sensing under stimulated breathing conditions: a kag-MOF based gas sensor as a case study

Materials Advances

ROYAL SOCIETY OF CHEMISTRY

COMMUNICATION

View Article Online
View Journal | View Issue

Check for updates

Cite this: *Mater. Adv.*, 2024, 5, 8432

Received 22nd April 2024,
Accepted 23rd June 2024

DOI: 10.1039/d4ma00417e

rsc.li/materials-advances

A non-invasive approach for H_2S gas sensing under stimulated breathing conditions: a kag-MOF based gas sensor as a case study†

Mostafa Zeama,[a] Jiangtao Jia,[a] Sheng Zhou,[a] Murilo Calil Faleiros,[b] Usman Yaqoob,[b] Osama Shekhah,[a] Khaled N. Salama *[b] and Mohamed Eddaoudi *[a]

Herein we report the deployment of kag-MOF as a sensing layer on a capacitive IDE sensor for detecting H_2S at room temperature. Compared to other gases such as nitrogen dioxide, ammonia, carbon dioxide, and carbon monoxide, kag-MOF exhibited a unique and selective response to H_2S, making it a promising candidate for H_2S sensing applications. In particular, the kag-MOF layer demonstrated a particularly good response and selectivity to H_2S in stimulated human breath and could detect concentrations as low as 500 ppb, even under humid conditions. These results clearly demonstrate that kag-MOF has immense potential as a candidate for H_2S sensing, and its sensing behaviour opens possibilities for developing gas/vapor sensors that could potentially diagnose uremia at an early stage by monitoring H_2S levels in the breath, giving it a potential application in the field of healthcare.

Introduction

Uremia is a medical condition that occurs when the kidneys are unable to efficiently filter out metabolic waste products from the bloodstream. The buildup of toxins in the body can cause serious health complications if not detected and treated early. This condition can be caused by a variety of factors, including viral infections, kidney damage, or certain medications.[1–4] When left untreated, uremia can cause fatigue, nausea, confusion, changes in urine properties, and in severe cases, the condition can lead to coma or even death.[5–7] As such, early detection of uremia is crucial for the effective management and prevention of further complications.

Fortunately, there are several methods available to detect uremia at an early stage. Medical tests such as blood, urine, and imaging tests, besides physical examination, can all be used to detect the presence of uremia. Interestingly, recent studies have shown that elevated levels of hydrogen sulfide (H_2S) in the breath may be an indicator of uremia.[8–10] The presence of any low concentration of H_2S (as low as 100 ppb)[11] in human breath means that there is a degree of malfunction of the kidneys, which indicates a degree of uremia. When kidneys fail to filter waste products from the blood, the levels of H_2S build up in the body as certain sulfur-containing compounds are broken down. This leads to a condition called halitosis of uremic origin, or "uremic breath".[12–14]

Monitoring H_2S levels in breath using gas/vapor sensors is a non-invasive technique that could help in the early diagnosis of uremia. These sensors detect physical changes caused by the diffusion of various gases in the sensing layer.[15–19] The interdigitated electrode (IDE) technology has emerged as a promising method for gas/vapor detection due to its high sensitivity, low cost, small size, and simplicity.[20–23] Sensors are prepared by depositing a sensing layer over the electrode surface, and this layer is a critical component of any chemical sensor as it captures analyte gases.[24,25] Among these electrodes, capacitive IDEs are particularly suitable for gas sensing because they consume less power.[26–30]

Porous materials like metal–organic frameworks (MOFs) and covalent organic frameworks (COFs) have garnered considerable attention in recent years for their potential applications in many fields like separation, catalysis and gas sensing.[31–37] The development of MOF-based gas sensors has several advantages over traditional sensors due to their high selectivity, sensitivity, stability, and ability to detect low concentrations of gases.[38–40] In addition, MOFs are easily tunable, allowing for the optimization of their properties for specific applications.[41–43] Therefore, the use of MOFs in gas sensing

[a] *Functional Materials Design, Discovery, and Development research group (FMD3), Advanced Membranes & Porous Materials Center, Division of Physical Sciences and Engineering King Abdullah University of Science and Technology, Thuwal 23955-6900, Saudi Arabia. E-mail: mohamed.eddaoudi@kaust.edu.sa*

[b] *Sensors Lab, Electrical Engineering Program, Division of Computer, Electrical and Mathematical Sciences and Engineering King Abdullah University of Science and Technology, Thuwal 23955-6900, Saudi Arabia. E-mail: khaled.salama@kaust.edu.sa*

† Electronic supplementary information (ESI) available. See DOI: https://doi.org/10.1039/d4ma00417e

applications, such as the detection of H_2S in human breath, has the potential to revolutionize the field of chemical sensing.

One of the good MOF candidates is **kag**-MOF-1 which is constructed by a single metal ion building block approach. It is formed by connecting Zn^{+2} metal ions with a tetrazole organic linker forming a 2-D structure with one dimensional channel and a small pore size. The presence of the tetrazole linker forms a high localized charge density, which affords access to a unique multifunctional MOF adsorbent suitable and ideal for the removal of acid gases (CO_2 and H_2S), dehydration, and BTX sieving. This MOF has emerged as a promising candidate for H_2S sensing, owing to its ability to uptake H_2S at low concentration and ambient pressure.[44]

In this study, we developed a sensing device for detecting low levels of H_2S in human breath using **kag**-MOF as the sensitive layer on the capacitive IDE.

Experimental section

Interdigitated electrode fabrication

The IDEs were fabricated using standard complementary metal oxide semiconductor (CMOS) processes. Firstly, a highly doped n-type silicon wafer underwent thermal growth of a thick (2 micrometers) SiO_2 layer. The Si/SiO_2 substrate was then patterned by spin-coating AZ5214 photoresist onto its surface. Afterward, the coated substrate was prebaked at a temperature of 110 °C for 2 minutes. The photoresist was subsequently exposed to UV light with a dose of 80 mJ cm^{-2} using a mask plate. Following the exposure, the photoresist was developed using AZ 726 developer for 1 minute before being cleaned in deionized (DI) water. Ti/Au electrodes were then sputtered, with thicknesses of 10 nm and 100 nm, respectively. The substrate underwent cleaning in an ultrasonic bath with acetone, followed by rinsing with isopropyl alcohol (IPA) and DI water.

kag-MOF synthesis

The **kag**-MOF was prepared according to our previous report with a modified procedure to get a nano-sheet morphology structure.[44] In general, tetrazole-5-ethylester (328 mg, 2 mmol) and 20 mL of H_2O were heated in a Teflon-lined autoclave to 120 °C for 24 h. After cooling to room temperature, a solution of $Zn(NO_3)_3{\cdot}6H_2O$ (297 mg, 1 mmol) in 20 mL water was added to the previous solution. The mixture was shaken for several minutes and held for 24 hours to get a white milk-like solution. The particles were centrifuged and washed with water and methanol.

To fabricate the sensing device, an ink was prepared by suspending 8 mg of **kag**-MOF in 8 ml of DMF and sonicated for 30 minutes. The resulting ink was then deposited on the IDE at 65 °C to allow for particle rearrangement. After the preparation, the electrode was found to be loaded with approximately 1 mg of the MOF material.

Activating MOF films is crucial to obtain a guest-free film prior to sensing signal measurements.[38,40] To achieve this, the MOF adsorbent was fully reactivated by heating it at 150 °C in an oven for 12 hours to remove any residual solvent or water present in the pores.

Material characterization

Powder X-ray diffraction (PXRD) measurements were carried out using a Bruker D8 ADVANCE X-ray diffractometer with Cu K_α radiation (λ = 1.54178 Å). TGA measurements were performed with TA Instruments Q500 apparatus; the samples were heated under an air atmosphere (flow, 25 cm^3 min^{-1}; heating rate, 5 °C min^{-1}). Low-pressure gas adsorption measurements were performed at relative pressures of up to 1 atm with a fully automated 3Flex high-resolution gas adsorption analyzer (Micromeritics). The bath temperature for the CO_2 adsorption measurements was controlled with an ethylene glycol/H_2O recirculating bath. Field emission scanning electron microscope (FE-SEM) images were taken on a Quattro Dual Beam microscope at an acceleration voltage of 10 kV.

Sensing experiment

The sensing experiment utilized a custom cell with IDE-loaded material connected to a KEYSIGHT E4980AL LCR meter. The cell was sealed, and gas flow (regulated by an Alicat mass flow controller) was set to 200 SCCM. The schematic of the overall sensing system setup is shown elsewhere.[24] System temperature was maintained at 24 °C with a Julabo EH-F33 water chiller. The experiment began by introducing dry compressed air to establish the reference capacitance (C_0) until stabilization (material activation). Subsequently, the tested gas was introduced until capacitance saturation. After each experiment, the IDE was heated to 120 °C to fully recover the H_2S molecules and to ensure the complete activation of the sensing layer before the next gas sensing trial. All the measurements were performed in dry air and at 24 °C except when mentioned otherwise.

Testing gas preparation

The tested gases, purchased with specific concentrations (H_2S: 100 ppm, NH_3: 100 ppm, NO_2: 100 ppm, CO: 1000 ppm, CO_2: 1000 ppm), were dry and balanced with N_2. Gas concentrations were regulated by mixing them with dry air using a mass flow controller set at a fixed total flow rate of 200 SCCM. For relative humidity measurement, compressed air was introduced into a water bubbler with temperature control *via* a water chiller, then mixed with dry air to adjust the relative humidity ratio.

Results and discussion

The coating layer exhibited a homogenous coverage and strong adhesion to the substrate. The MOF film's purity and crystallinity were validated by comparing its powder X-ray diffraction (PXRD) pattern with the simulated pattern (Fig. 1B).[44] The film displayed excellent crystalline quality, featuring miniature two-dimensional sheets approximately 150 nm in size and well-mixed microcrystals with slight gaps in between, producing a consistent and dense MOF coating (Fig. 1C). The successful deposition of the MOF thin film onto the IDE substrate enabled us to use it for sensing permittivity alterations triggered by gas/vapor sorption.

Gas sensing application in dry conditions

We examined the sensing properties of the **kag**-MOF film on capacitive IDEs for a range of gases, including H_2S, NH_3, NO_2,

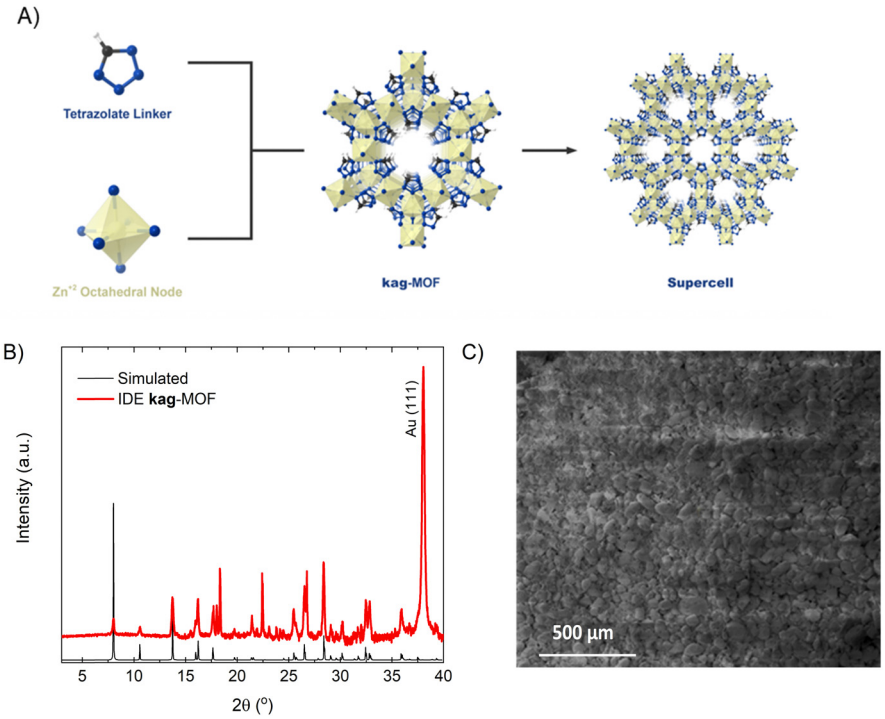

Fig. 1 (A) Simplified schematic representation of the **kag**-MOF showing the channel pore nature and the overall **kag** topology from the supercell. (B) PXRD of the **kag**-MOF film compared with the calculated PXRD from the CIF file. (C) The SEM image of the **kag**-MOF film.

CO_2, and CO. Gas sensing experiments were conducted using a fully automated measurement system with LabVIEW.[21] The coated sensor was placed inside a custom-built detection chamber and connected to an LCR meter to measure changes in capacitance.

To prepare for each cycle of analyte exposure, the sensor was heated up to 120 °C using an *in situ* heating system in a homemade gas chamber. The temperature of the heater output was calibrated using a Micro radiometric thermal imaging microscope, which measures and displays the temperature distribution over the surface of small devices.[45] This calibration is crucial to maintain the integrity of the MOF thin film and ensure that we have a guest-free activated **kag**-MOF before conducting sensing experiments.[44] The sensing performance and characteristics of **kag**-MOF were evaluated at various H_2S concentrations in both dry and humid conditions to assess the potential application of the newly developed sensor.

The sensor shows different responses across a wide range of H_2S concentrations (from 0.5 to 100 ppm), it was observed that at higher concentration, the device reveals a linear response while at low concentration (<1 ppm) its slope changes. The capacitance can be determined using the standard capacitance equation.[46] The change in capacitance is attributed to the dielectric constant dependency of the IDE's capacitive properties

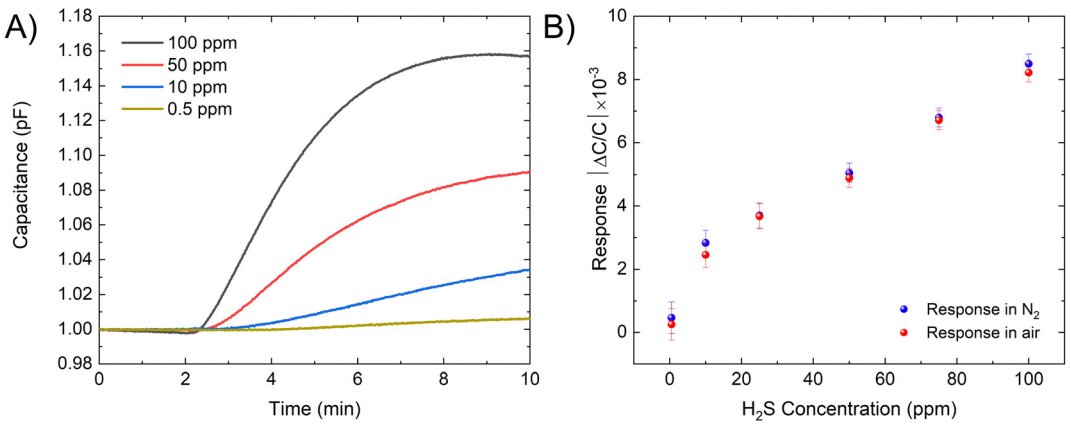

Fig. 2 (A) Capacitive sensor response for **kag**-MOF in the presence of different concentration of H_2S. (B) The response of the sensor for different H_2S concentrations.

on the concentration of H_2S. This is because H_2S interaction with **kag**-MOF affects the local dielectric properties of the film. Therefore, exposure of the sensor to varying dry H_2S concentrations results in an increase in capacitance. As depicted in Fig. 2, the sensor exhibits a good response at a low concentration of H_2S (0.5 ppm), which makes it a suitable candidate for trace-level H_2S detection. The sensor's response was assessed in both N_2 and air atmospheres, revealing comparable responses in both environments (within the measurement's error range). This suggests that the sensor's reaction to various gases in the air mixture is negligible. Furthermore, the material demonstrates notable stability under both air and humid conditions.[44]

As the stability and repeatability of a sensing device are crucial for its effectiveness. The stability of the device was assessed by exposing it to 100 ppm of H_2S for 7 consecutive cycles. The device was activated *in situ* by heating it to 120 °C for five minutes and then allowing it to cool down under an air environment for 20 minutes. The detection levels were shown to be stable and uniform across all cycles. To assess the long-term stability of the sensor, cyclic exposure to 100 ppm of H_2S was performed at room temperature every 24 hours for a period of 14 days. As depicted in Fig. 3, the results revealed that the sensor response remained consistent over time, indicating its long-term stability. The crystallinity of the sensing layer was further confirmed by comparing the PXRD patterns before and after the sensing experiment [Fig. SI, ESI†]. The results showed that the MOF retained its crystallinity, which confirms the stability of the film under the sensing conditions.

Based on our sensing data and IDE stability analysis, we conducted further investigations to determine the selectivity of the sensor for H_2S. To assess the sensor's selectivity, we evaluated its response to other gases at different concentrations. The results showed that the **kag**-MOF sensor had exceptional selectivity for H_2S compared to other tested gases. Although the sensor displayed some response to gases such as ammonia (NH_3), nitrogen dioxide (NO_2), carbon dioxide (CO_2), and carbon monoxide (CO), the signals produced were minor. Notably, NH_3 and NO_2 generated the most significant signals, whereas CO_2 and CO produced nearly negligible signals, as illustrated in Fig. 4. Furthermore, the H_2S signal was approximately nine times higher than that of NH_3, indicating the sensor's high selectivity for H_2S over other tested gases with distinct physical and chemical properties.

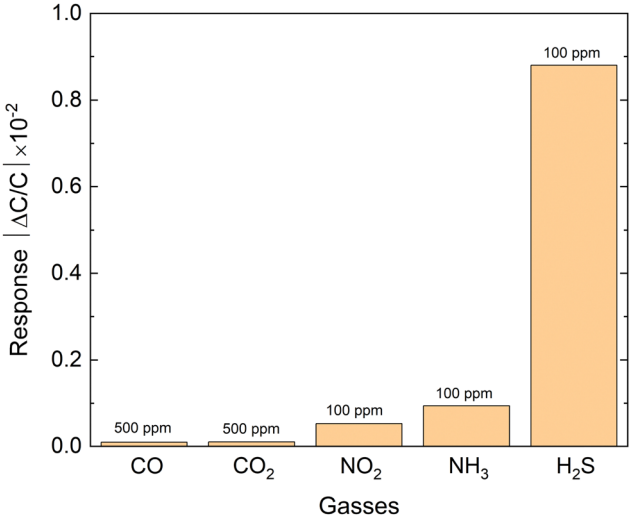

Fig. 4 Selectivity of the **kag**-MOF sensor to hydrogen sulfide (H_2S), ammonia (NH_3), nitrogen dioxide (NO_2), carbon dioxide (CO_2), and carbon monoxide (CO) at different concentrations.

Sensing mechanisms

The gas sensing response is driven by dipole interaction between physiosorbed gas and the MOF. Material characterization revealed a strong affinity of the MOF for H_2S.[44] DFT calculations were employed to understand the sensing mechanism and gas response disparity between H_2S and NH_3. Both gases were found to be adsorbed on the tetrazole ring in the pore, with calculated adsorption energy of 50 kJ mol^{-1} for H_2S and 40 kJ mol^{-1} for NH_3. Charge analysis showed a partial negative charge on S and N in H_2S and NH_3, respectively. The discrepancy in adsorption energy is attributed to a partial positive charge on the adsorbed MOF region, with charges of $-2.4e$ and $-1.3e$ on S and N, respectively. As system

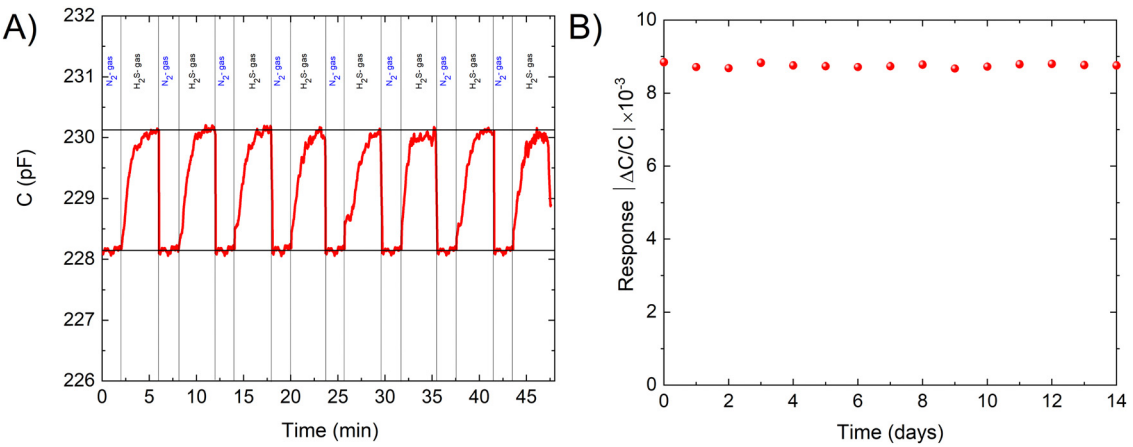

Fig. 3 (A) The recyclability of the sensor in the presence of 100 ppm of H_2S. (B) The response of the sensor for 100 ppm H_2S measured daily for 2 weeks.

capacitance is charge-dependent, it varies with different gases, affecting the gas response. The greater affinity of **kag**-MOF for H_2S, indicated by the difference in binding energy, explains the difference in response. This sensing mechanism is generalized for various tested gases physiosorbed on the framework.

Relative humidity response

Environmental moisture can significantly affect the gas sensor response, as capacitive sensor technology is based on the film's dielectric changes caused by gas/vapor sorption, it is often criticized for being sensitive to humidity.[46] In practice, water vapor and condensable vapours can significantly affect IDE-based sensors since water has a much larger dielectric constant (ε_r = 80) than H_2S (ε_r = 5.8), which can interfere with the IDE sensory signal of H_2S.[47,48] Consequently, the presence of moisture can hinder the qualitative identification and quantification of H_2S.

We therefore investigated the concentration-dependent response of the IDE device coated with **kag**-MOF under humid conditions (Fig. 5). Our findings revealed that the presence of moisture had a substantial impact on the **kag**-MOF coated IDE sensors. In order to gain a better understanding of the sensing performance of water vapor adsorption, a detailed analysis of the response toward H_2O was conducted as a function of relative humidity (RH), ranging from 5% to 90% RH. The sensor was activated at 120 °C and then exposed to varying levels of RH using dry compressed air as a carrier gas. The RH level was adjusted by changing the carrier flow (0–200 mL min^{-1}) through water bubbling. The **kag**-MOF coated IDE sensor demonstrated a good response to humidity levels in a nonlinear fashion, as shown in Fig. 5A. These results are consistent with the dehydration ability of **kag**-MOF, which has a high affinity for water molecules due to its contracted pore system and localized high charge density and supported by its hydrolytic stability.[44]

Effect of humidity on H_2S sensing

To evaluate the influence of humidity on the sensor's response toward H_2S, we conducted a test to measure the sensor's response to H_2S in a humid environment with a different relative humidity (5–90%). The introduction of H_2S gas resulted in a reduction in the sensor's capacitance. However, the sensor's response for H_2S was improved by a factor of 10, as shown in Fig. 5B. The decrease in capacitance suggests that **kag**-MOF experiences a partial desorption of non-coordinated water molecules due to their competition with H_2S molecules.[44,49]

The impact of relative humidity (RH) on the **kag**-MOF sensor's performance was investigated. The sensor was activated at 120 °C and exposed to varying RH levels using dry compressed air as a carrier gas. The RH was adjusted by modifying the carrier flow (0–200 mL min^{-1}) through water bubbling. The chamber's humidity was set to the desired level (from dry air up to 90% RH), and the capacitance response was considered as the new baseline (Fig. S9, ESI†). At each RH level, a capacitance change was recorded in the presence of 50 ppm H_2S (Fig. 5C). It was observed that the response is nearly similar to that for dry H_2S up to 30% RH (Fig. 2B). Then, an increase in the sensor response with an increase in RH up to 50% RH is attributed to the dissolution of H_2S molecules into the physiosorbed water on the **kag**-MOF layer. This is due to the fact that **kag**-MOF is known based on water sorption studies to become saturated with water above 30% RH.[44]

H_2S response in simulated human exhale

Based on the previous results, we proposed that the **kag**-MOF has potential for detecting H_2S in human exhaled breath based on our studies. Since the humidity level in human breath falls within the range of 5% to 6.3%, we conducted tests to evaluate the sensor's response to human breath by exposing the IDE electrode to a gas mixture of 78% N_2, 13% O_2, and 4% CO_2 with a humidity of 5% to mimic the conditions of human exhalation.[50] Subsequently, various concentrations of H_2S (10–40 ppm) were introduced, and the outcomes are presented in Fig. 6. The capacitance of the electrode increased non-linearly with increasing H_2S concentration, indicating good response to H_2S in human breath. The sensor's response to H_2S in air was found to be comparable to its response in simulated human breath due to the low water concentration, and the negligible response to CO_2 and O_2 with respect to H_2S.

Volatile organic compounds (VOCs) such as formaldehyde usually coexist with other gases in human breath in the case of uremia. The selectivity of the sensor to formaldehyde (as one of

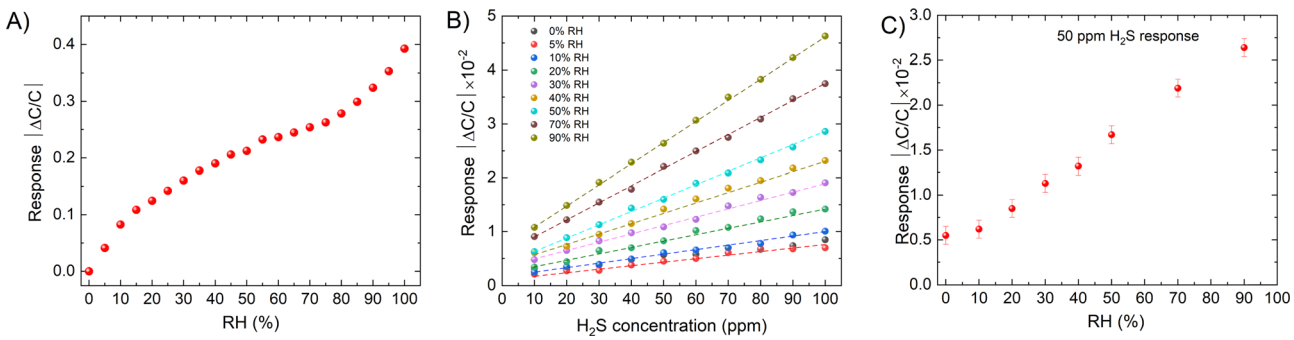

Fig. 5 (A) Response of the **kag**-MOF to different relative humidity ratios. (B) Response of the sensor to H_2S in the presence of different RH. (C) Response of the sensor to 50 ppm H_2S at different relative humidity (RH).

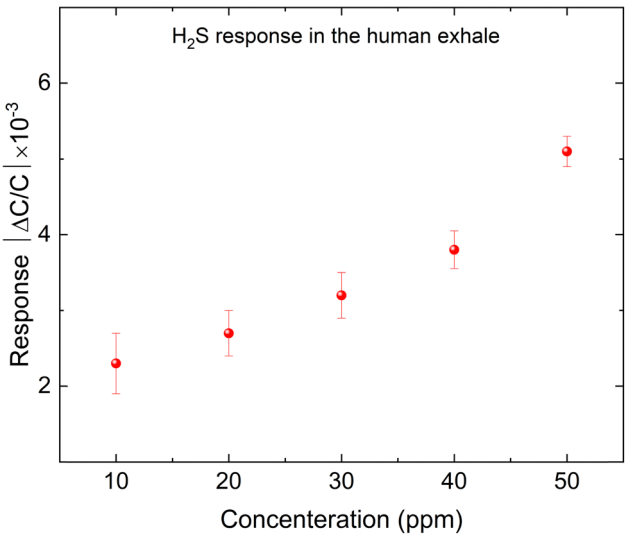

Fig. 6 Response of the sensor to H_2S in the presence of human exhale mixture.

the VOCs) is studied. Human exhaled air contains formaldehyde in concentrations ranging from 0.001 to 0.01 mg m^{-3}, with an average value of about 0.005 mg m^{-3}, equivalent to approximately 0.00774017 ppm.[51–53] However, due to system limitations, we could not achieve this concentration in our experiment. Therefore, we tested the sensor at a 1 ppm concentration of formaldehyde (FA) under different humid conditions, as human breath is humid. Additionally, we tested 1 ppm FA at 5% RH with varying concentrations of H_2S. The results (Fig. S10 and S11, ESI†) show that the sensor material has almost no sensitivity to FA in both tests. Therefore, there is no cross-sensitivity that could affect the sensor's performance.

Conclusion

In conclusion, this study showed the successful deployment of **kag**-MOF as a sensing layer on a capacitive IDE sensor for H_2S detection at room temperature. The MOF layer could detect H_2S concentrations as low as 500 ppb, even under humid conditions. The MOF sensor demonstrated good response and selectivity to H_2S in human breath, and its stability was confirmed by various methods, demonstrating its greater chemical stability. Moreover, **kag**-MOF exhibited a unique and selective response to H_2S compared to other gases such as nitrogen dioxide, ammonia, carbon dioxide, and carbon monoxide. This sensing behaviour of **kag**-MOF opens possibilities for developing gas/vapor sensors for the early detection of uremia. By monitoring H_2S levels in the breath, healthcare professionals could potentially diagnose uremia at an early stage, which is crucial for the effective management and prevention of complications. However, it is essential to note that while gas/vapor sensors are a promising tool, they should not be used in isolation and should be used in conjunction with other diagnostic tests, such as blood and urine tests, to ensure accurate diagnosis.

Data availability

Data supporting this study are included within the article and/or supporting materials.

Conflicts of interest

There are no conflicts to declare.

Acknowledgements

The authors acknowledge the King Abdullah University of Science and Technology for funding this project.

References

1 T. W. Meyer and T. H. Hostetter, *N. Engl. J. Med.*, 2007, **357**, 1316–1325.
2 G. A. Kaysen, *J. Am. Soc. Nephrol.*, 2001, **12**, 1549–1557.
3 M. Schömig, A. Eisenhardt and E. Ritz, *Blood Purif.*, 2000, **18**, 327–332.
4 D. Ormrod and T. Miller, *Nephron*, 2008, **26**, 249–254.
5 C. K. Yeung, D. D. Shen, K. E. Thummel and J. Himmelfarb, *Kidney Int.*, 2014, **85**, 522–528.
6 A. I. Arieff, S. G. Massry, A. Barrientos and C. R. Kleeman, *Kidney Int.*, 1973, **4**, 177–187.
7 D. J. Prezant, *Lung*, 1990, **168**, 1–14.
8 E. Levine, *Urol. Radiol.*, 1991, **13**, 203–210.
9 H. Uchida, N. Kiyokawa, H. Horie, J. Fujimoto and T. Takeda, *Pediatr. Res.*, 1999, **45**, 133–137.
10 T. W. Meyer and T. H. Hostetter, *J. Am. Soc. Nephrol.*, 2014, **25**, 2151–2158.
11 H. E. Bass and E. Singer, *J. Am. Med. Assoc.*, 1950, **144**, 819–823.
12 A. Manolis, *Clin. Chem.*, 1983, **29**, 5–15.
13 M. L. Simenhoff, J. F. Burke, J. J. Saukkonen, A. T. Ordinario, R. Doty and S. Dunn, *N. Engl. J. Med.*, 1977, **297**, 132–135.
14 N. Pagonas, W. Vautz, L. Seifert, R. Slodzinski, J. Jankowski, W. Zidek and T. H. Westhoff, *PLoS One*, 2012, **7**, e46258.
15 P. Bindra and A. Hazra, *J. Mater. Sci.: Mater. Electron.*, 2018, **29**, 6129–6148.
16 D. J. Wales, J. Grand, V. P. Ting, R. D. Burke, K. J. Edler, C. R. Bowen, S. Mintova and A. D. Burrows, *Chem. Soc. Rev.*, 2015, **44**, 4290–4321.
17 J. R. Stetter, W. R. Penrose and S. Yao, *J. Electrochem. Soc.*, 2003, **150**, S11.
18 L. Zhang, P. De Schryver, B. De Gusseme, W. De Muynck, N. Boon and W. Verstraete, *Water Res.*, 2008, **42**, 1–12.
19 O. Yassine, O. Shekhah, A. H. Assen, Y. Belmabkhout, K. N. Salama and M. Eddaoudi, *Angew. Chem., Int. Ed.*, 2016, **55**, 15879–15883.
20 F. J. Pavinatto, C. W. Paschoal and A. C. Arias, *Biosens. Bioelectron.*, 2015, **67**, 553–559.
21 V. Tsouti, C. Boutopoulos, I. Zergioti and S. Chatzandroulis, *Biosens. Bioelectron.*, 2011, **27**, 1–11.

22 F. J. Pavinatto, C. W. A. Paschoal and A. C. Arias, *Biosens. Bioelectron.*, 2015, **67**, 553–559.
23 U. Yaqoob and M. I. Younis, *Journal*, 2021, 21.
24 C. Sapsanis, H. Omran, V. Chernikova, O. Shekhah, Y. Belmabkhout, U. Buttner, M. Eddaoudi and K. N. Salama, *Journal*, 2015, **15**, 18153–18166.
25 E. Llobet, *Sens. Actuators, B*, 2013, **179**, 32–45.
26 M. Kitsara, D. Goustouridis, S. Chatzandroulis, M. Chatzichristidi, I. Raptis, T. Ganetsos, R. Igreja and C. J. Dias, *Sens. Actuators, B*, 2007, **127**, 186–192.
27 C. Berggren, B. Bjarnason and G. Johansson, *Electroanalysis*, 2001, **13**, 173–180.
28 A. M. Kummer and A. Hierlemann, *IEEE Sens. J.*, 2006, **6**, 3–10.
29 U. Yaqoob, W. B. Lenz, N. Alcheikh, N. Jaber and M. I. Younis, *IEEE Sens. J.*, 2022, **22**, 19858–19866.
30 U. Yaqoob, N. Jaber, N. Alcheikh and M. I. Younis, *Sci. Rep.*, 2022, **12**, 5297.
31 H.-C. Zhou, J. R. Long and O. M. Yaghi, *Journal*, 2012, **112**, 673–674.
32 R. J. Kuppler, D. J. Timmons, Q.-R. Fang, J.-R. Li, T. A. Makal, M. D. Young, D. Yuan, D. Zhao, W. Zhuang and H.-C. Zhou, *Coord. Chem. Rev.*, 2009, **253**, 3042–3066.
33 H. Furukawa, K. E. Cordova, M. O'Keeffe and O. M. Yaghi, *Science*, 2013, **341**, 1230444.
34 V. Chernikova, O. Shekhah, Y. Belmabkhout, M. Karunakaran and M. Eddaoudi, *Angew. Chem.*, 2023, **135**, e202218842.
35 P. T. Parvatkar, S. Kandambeth, A. C. Shaikh, I. Nadinov, J. Yin, V. S. Kale, G. Healing, A.-H. Emwas, O. Shekhah, H. N. Alshareef, O. F. Mohammed and M. Eddaoudi, *J. Am. Chem. Soc.*, 2023, **145**, 5074–5082.
36 M. Zeama, M. A. Morsy, M. Abdelnaby, L. Gutiérrez-Arzaluz, O. F. Mohammed and Z. H. Yamani, *Chem. – Asian J.*, 2021, **16**, 2520–2528.
37 M. Zeama, M. Morsy, S. Abdel-Azeim, M. Abdelnaby, A. Alloush and Z. Yamani, *Inorg. Chim. Acta*, 2020, **501**, 119287.
38 S. Achmann, G. Hagen, J. Kita, I. M. Malkowsky, C. Kiener and R. Moos, *Journal*, 2009, **9**, 1574–1589.
39 M. Drobek, J.-H. Kim, M. Bechelany, C. Vallicari, A. Julbe and S. S. Kim, *ACS Appl. Mater. Interfaces*, 2016, **8**, 8323–8328.
40 C. Arul, K. Moulaee, N. Donato, D. Iannazzo, N. Lavanya, G. Neri and C. Sekar, *Sens. Actuators, B*, 2021, **329**, 129053.
41 L. E. Kreno, K. Leong, O. K. Farha, M. Allendorf, R. P. Van Duyne and J. T. Hupp, *Chem. Rev.*, 2012, **112**, 1105–1125.
42 D.-X. Xue, Y. Belmabkhout, O. Shekhah, H. Jiang, K. Adil, A. J. Cairns and M. Eddaoudi, *J. Am. Chem. Soc.*, 2015, **137**, 5034–5040.
43 J. H. Choi, Y. J. Choi, J. W. Lee, W. H. Shin and J. K. Kang, *Phys. Chem. Chem. Phys.*, 2009, **11**, 628–631.
44 M. I. H. Mohideen, R. S. Pillai, K. Adil, P. M. Bhatt, Y. Belmabkhout, A. Shkurenko, G. Maurin and M. Eddaoudi, *Chem*, 2017, **3**, 822–833.
45 G. Bieszczad and M. Kastek, *Metrol. Meas. Syst.*, 2011, **18**, 679–690.
46 W. C. Heerens, *J. Phys. E: Sci. Instrum.*, 1986, **19**, 897.
47 S. Havriliak, R. Swenson and R. Cole, *J. Chem. Phys.*, 1955, **23**, 134–135.
48 G. Oster and J. G. Kirkwood, *J. Chem. Phys.*, 1943, **11**, 175–178.
49 A. Cadiau, Y. Belmabkhout, K. Adil, P. M. Bhatt, R. S. Pillai, A. Shkurenko, C. Martineau-Corcos, G. Maurin and M. Eddaoudi, *Science*, 2017, **356**, 731–735.
50 G. Ejaimi and S. Saeed, *Ann. Int. Med. Den. Res.*, 2016, **3**, 1.
51 I. Kushch, K. Schwarz, L. Schwentner, B. Baumann, A. Dzien, A. Schmid, K. Unterkofler, G. Gastl, P. Spaněl, D. Smith and A. Amann, *J. Breath Res.*, 2008, **2**, 026002.
52 B. Moser, F. Bodrogi, G. Eibl, M. Lechner, J. Rieder and P. Lirk, *Respir. Physiol. Neurobiol.*, 2005, **145**, 295–300.
53 A. Wehinger, A. Schmid, S. Mechtcheriakov, M. Ledochowski, C. Grabmer, G. A. Gastl and A. Amann, *Int. J. Mass Spectrom.*, 2007, **265**, 49–59.